J Ther Eng, Vol. 10, No. 2, pp. 350−359, March, 2024

Journal of Thermal Engineering
Web page info: https://jten.yildiz.edu.tr
DOI: 10.18186/thermal.1448621

Journal of Thermal Engineering

Research Article

Numerical analysis of Turbulent flow and heat transfer enhancement using V-shaped Grooves mounted on the Rotary Kiln's outer Walls

Youcef ATTOU[1], Mohamed BOUHAFS[1], Abdelkader FEDDAL[2]

[1]*Institute of Maintenance and Industrial Safety, University of Mohamed Ben Ahmed Oran, 31000, Algeria*
[2]*Faculty of Mechanical Engineering, University of Sciences and Technology, Oran, 1505, Algeria*

ARTICLE INFO

Article history
Received: 20 October 2022
Revised: 19 January 2023
Accepted: 08 February 2023

Keywords:
Heat Transfer Enhancement; K -Ω Sst Model; Rotary Ciment Kiln; V-Shaped Groove

ABSTRACT

Rotary kilns have been widely employed in various industrial uses, especially the cement production. This article deals with enhancing the thermal performance of a rotary kiln duct with V-shaped grooves mounted on the outer wall. Four V-shaped grooves with different depths h/D ranging from 0.1 to 0.4 were designed. The Reynolds Averaged Navier–Stokes equations (RANS) of two-dimensional steady-state flow are used to model the governing flow equations by using the finite volume approach (FVM) in FLUENT. *k*-ε standard, *k*-ε Realizable, *k*-ω SST and *k*-ε RNG turbulence models of the RANS approach and the *k* -ω SST model has been adopted to validate CFD results. In this study, the numerical results have revealed that the increase in groove depth decrease the temperature of the rotary kiln's outer wall than the smooth walls and gives the largest Nu number, especially for the groove with h/D =0.3 and 0.4 depths.

Cite this article as: Attou Y, Bouhafs M, Feddal A. Numerical analysis of Turbulent flow and heat transfer enhancement using V-shaped Grooves mounted on the Rotary Kiln's outer Walls. J Ther Eng 2024;10(2):350−359.

INTRODUCTION

Algeria's cement industry has gradually improved in recent years as the number of cement production lines has increased. The rotary kiln is the primary piece of equipment used in cement production, from limestone calcination to cement manufacturing. It is a type of heat exchanger that consists of a steel tube lined with refractory brick. The rotary kiln rotates at 0.5 to 5 revolutions per minute and is inclined from 1 to 4 degrees. The rotary kiln is divided into four sections [1]: Preheating/drying, calcining /decomposition, burning, cooling (Figure 1).

The heat transfer phenomenon in a rotary kiln is complicated because it includes conduction, convection, and radiation all at the same time. Many researchers investigated the heat transfer mechanism in refractory kilns, as shown in [2,3]. Sass [4] created a heat transfer model for rotary kiln dryer radiation transfer calculations using empirical relations. Ghoshdastidar et al. [5] created a heat transfer model for a wet iron ore heating rotary kiln. This model was accurate in terms of kiln length, axial solid and gas temperatures. Ghoshdastidar and Agarwal [6] also conducted a numerical study of heat exchange in a rotary kiln for drying and preheating wood chips. Schmidt and

*Corresponding author.
*E-mail address: attou_youcef@yahoo.com

This paper was recommended for publication in revised form by Editor-in-Chief Ahmet Selim Dalkılıç

Nikrityuk [7] conducted a two-dimensional (2D) numerical simulation of transient heat transfer in a horizontal rotary kiln using DNS. They demonstrated that the gas vortex enhanced convective heat transfer in the top of the particulate bed. Sonavane and Specht [8] performed a numerical simulation using the Finite Element Method (FEM) to predict temperature fluctuations in the rotary kiln wall. In addition, Cook and Cundy [9] created a mathematical model to predict heat transfer between a rotating cylinder's heated wall and an adjacent wet granular medium. Elattar et al. [10,11] used a two-dimensional (2D) CFD simulation to investigate the impact of rotary kiln operating conditions and burner geometrical parameters on flame characteristics such as heat and fluid flow when using gaseous fuels. They also investigated the effects of primary air ratio, burner geometry on the flow field, and kiln wall peak temperature.

Mirhosseini et al. [12] recently investigated numerically the influence of an absorber placed around a rotary kiln on heat transfer characteristics. As a future study, the absorber is specifically designed for heat recovery. They discovered that the contribution of radiative heat transfer to the total heat transferred from the kiln to the absorber is significant.

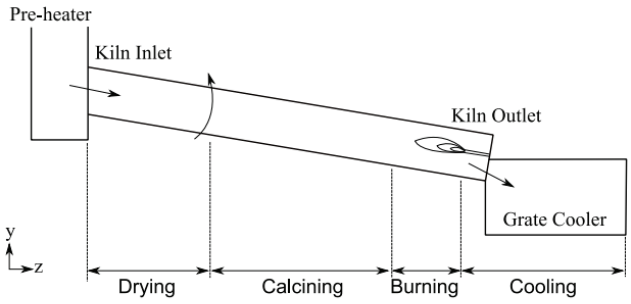

(a) Schematic of rotary cement kiln showing key regions

Figure 1. Figure 1. Schematic view of the rotary cement kiln [29]. Adapted from: Csernyei C, Christopher M. Numerical Modelling of a Rotary Cement Kiln with External Shell Cooling Fans. Electronic Thesis and Dissertation Repository. 2016. Available at: https://ir.lib.uwo.ca/etd/3682.

A few studies have been conducted to investigate jet impingement cooling of circular cylinders [13,14]. Csernyei et al. [15] conducted a numerical investigation to study the convective heat exchange caused by multiple circular jets impinging on a horizontal cylinder, as evidenced by the cooling of rotary cement kilns using large axial fans. The effect of changing the geometric parameters of the shell cooling fans on the kiln's shell temperature was also investigated. Grooved channels, which are the major components in annular spaces, are widely used in industrial applications to improve heat transfer [16-18]. Nouri-Borujerdi et al. [19,20] provide comprehensive reviews of rotating cylinder cooling. These reviews are primarily concerned with the cooling of grooved cylinders. More recently, Moumin et al. [21] conducted an experimental study of heat transfer to the bed inside a rotary kiln. They used sand as a granular material and cement raw meal as a powdery material, as well as a rotating cylinder with rotational speeds of 1, 2, and 3 rpm heated through the outer shell.

Many experimental and numerical studies on thermal performance enhancement using V-shaped fins, such as heat exchangers, turbines, impingement cooling, and solar air receiver/heater have been widely conducted [30-32]. Promvonge et al. [33] carried out an experimental study to investigate thermal behaviors in a heat exchanger channel with V-shaped ribs and grooves. They discovered that the thermal enhancement factor (TEF) is around 2.12, 2.14, and 2.11, indicating that the baffle-groove performs better than the rib-groove by about 13%. Kaur et al. [34] investigated numerically the effect of six V-rib configurations on thermal-hydraulic performance in a square channel. They found that the mean heat transfer and pressure drop values of compound 'V-rib and V-protrusion' configurations provided the best thermal-hydraulic performance value and the highest Nusselt number ratio at a fixed Reynolds number of 50,000.

The temperature increases outside the furnace in the case of the failure of furnace refractory bricks by crusting, bricks wear (where it exceeds 650°C) and therefore influences the behavior

Figure 2. Deformation of the outer wall of the rotary cement kiln.

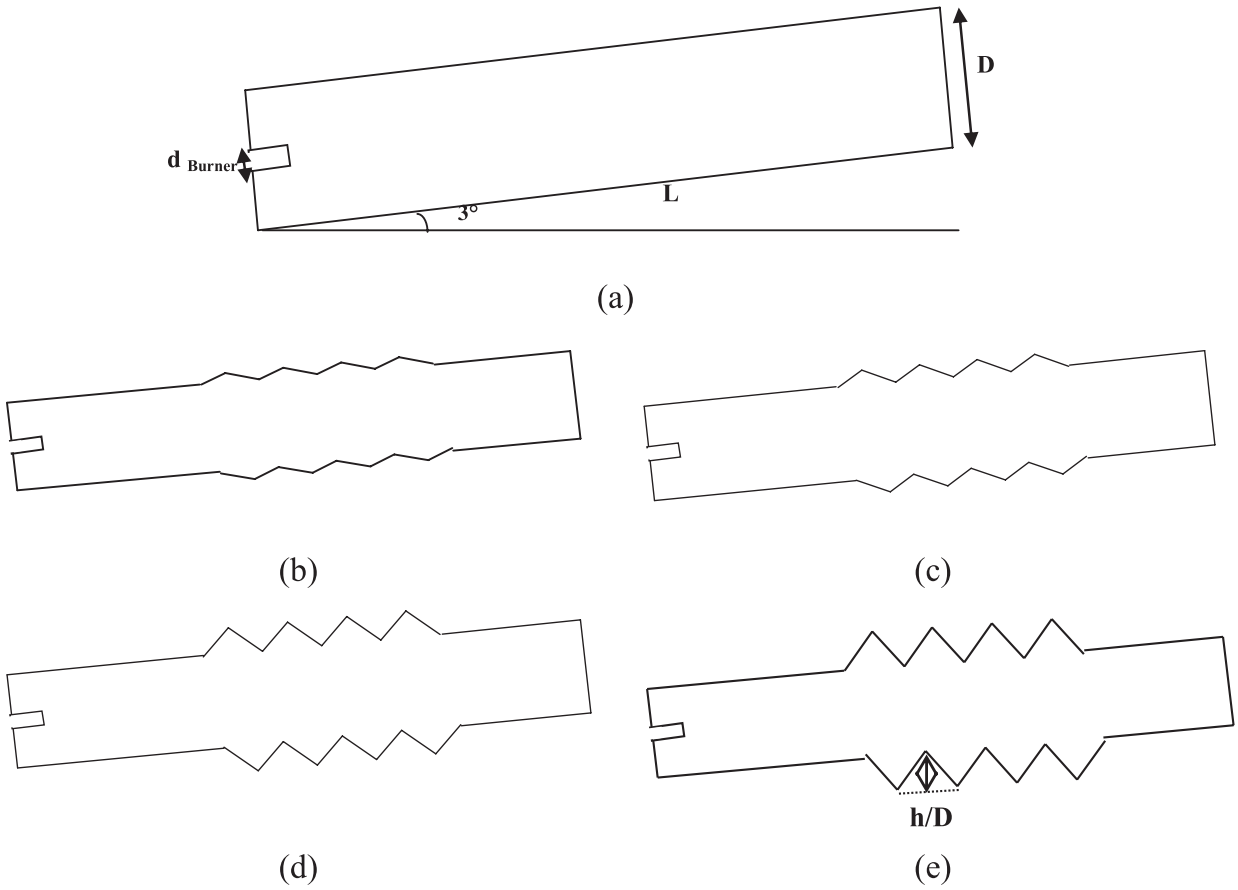

Figure 3. Two-dimensional model of rotary kiln: (a) Smooth walls, (b) grooved wall with h/D=0.1, (c) grooved wall with h/D=0.2, (d) grooved wall with h/D=0.3, (e) grooved wall with h/D= 0.4.

of the shell material (Figure 2). The use of V-shaped grooves mounted on rotary kiln's outer wall has been no reported in any research article. The purpose is to analyze the variation of the depth of grooves with different depth ratio from 0.1 to 0.4 on the heat transfer intensification in rotary kilns.

PROBLEM STATEMENT

Figure 3 depicts a schematic representation of a two-dimensional grooved wall with depths (h/D) ranging from 0.1 to 0.4. The type of rotary cement kin used in this research, from Lafarge Cement Plant [22] which is located in Oggaz (Wilaya of Mascara, Algeria). The kiln diameter D and length L were 5 and 40 meters, respectively, and d is the diameter of the burner. Rotary kiln is titled of 3 degrees. Furthermore, the V-shaped grooves are installed on the kiln's burning wall to improve heat exchange and protect the outer cylinder.

Simulation Procedure and Governing Equation

ANSYS FLUENT is used in this work to numerically solve the governing equations (Patankar and Spalding [23]), and the convective terms are solved using a second order upwind scheme. The SIMPLE algorithm, on the other hand, is used for velocity-pressure coupling. The residuals lower than 10^{-6} is chosen to achieve the convergence criterion for all variables [24].

The governing conservation equations for air flow and heat transfer inside the rotary kiln are as follows:

Continuity Equation

$$\frac{\partial u_j}{\partial x_j} = 0 \tag{1}$$

Movement Quantity Equation

$$\rho U_j \frac{\partial}{\partial x_j}(U_i) = -\frac{\partial P}{\partial x_j} + \mu \frac{\partial^2 u_i}{\partial x^2{}_j} + \underbrace{\frac{\partial}{\partial x_j}\left(-\rho \overline{u_i' u_j'}\right)}_{\text{Constraints of Reynolds}} + \rho g_i \tag{2}$$

Energy Equation

$$\frac{\partial}{\partial x_j}\left(\rho U_j T\right) = \frac{\lambda}{Cp}\frac{\partial^2 T}{\partial x^2{}_j} + \frac{\partial}{\partial x_j}\left(-\overline{\rho u_j' t_p'}\right) \tag{3}$$

All of these equations have the following general form:

$$\underbrace{\frac{\partial\left(\rho u_j \phi\right)}{\partial x_j}}_{1} = \underbrace{\frac{\partial}{\partial x_j}\left(\Gamma_\phi \frac{\partial \phi}{\partial x}\right)}_{2} + \underbrace{S_\phi}_{3} \tag{4}$$

Term 1: transport of ϕ by convection.
Term 2: transport of ϕ by diffusion.
Term 3: local production of ϕ.

The local Nusselt number is displayed along the grooved kiln wall as follows:

$$Nu = \frac{h\, D_h}{\lambda_{iar}} \tag{5}$$

Turbulence and Mathematical Models

In this study, four turbulence models (RANS approach) were tested: *k*-ε standard, *k*-ε Realizable, *k*-ω SST and *k*-ε RNG. According to the findings, the *k*-ω SST model is more accurate than the others in validating CFD results. The Menter [25] k- SST (Shear Stress Transport) model is used to treat turbulence. This model combines two models: Wilcox's [26] *k*-ω model for the area close to the wall and Jones and Launder's [27] standard *k*-ε model for the area far from the wall. Under adverse pressure gradients, the k-ω SST model provides highly accurate predictions of the beginning and amount of flow separation (Bardina et al. [28]). It is recommended for high accuracy boundary layer simulations, making it the ideal model for the current simulation. The k and ω transport equations of SST turbulence model are:

$$\frac{\partial(\rho k)}{\partial t} + \frac{\partial(\rho U_j k)}{\partial x_j} = \widetilde{P}_k - \beta^* \rho k \omega + \frac{\partial}{\partial x_j}\left(\Gamma_k \frac{\partial k}{\partial x_j}\right) \tag{6}$$

$$\frac{\partial(\rho\omega)}{\partial t} + \frac{\partial(\rho U_j \omega)}{\partial x_j} = \frac{\gamma}{\nu_t} P_k - \beta\rho\omega^2 + \frac{\partial}{\partial x_j}\left(\Gamma_\omega \frac{\partial \omega}{\partial x_j}\right) + 2\rho\sigma_{\omega 2}\frac{1}{\omega}\frac{\partial k}{\partial x_j}\frac{\partial \omega}{\partial x_j} \tag{7}$$

With:

P_k represents production of turbulent kinetic energy due to the gradient of the average velocity:

$$\Gamma_k = \mu + \frac{\mu_t}{\sigma_k};\ \Gamma_\omega = \mu + \frac{\mu_t}{\sigma_\omega};\ P_k = \tau_{ij}\frac{\partial U_i}{\partial x_j};\ \widetilde{P}_k = \min(P_k, C_{1\varepsilon}) \tag{8}$$

$$\overline{u_i u_j} = \frac{2}{3}k\delta_{ij} - \nu_t S_{ij} \tag{9}$$

Where ν_t is turbulent kinematic viscosity computed by combining k and ε:

$$\nu_t = c_\mu f_\mu \frac{k^2}{\varepsilon} \tag{10}$$

With the mean strain rate tensor, *Sij*, defined as

$$S_{ij} = \left(\frac{\partial U_i}{\partial x_j} + \frac{\partial U_j}{\partial x_i}\right) \tag{11}$$

Boundary Conditions and Grid Distribution

The computational domain's boundary conditions were primary and secondary air velocities, the temperature of the rotary kiln's outer wall and air is considered as the working fluid (Figure 4). The following boundary conditions are appropriate for this study: primary air velocity of 23.3m/s at 1573 K, secondary air velocity of 2.35m/s at 373 K. Thereafter, the constant wall temperature is then applied and the kiln rotational speed is set to 4 rpm (≈0.42 rad/s).

In our study, we used the 2D channel without and with V-shaped grooves, and simulations were performed using the mesh generated in ANSYS ICEM as a preprocessing program with structured mesh (hexahedral mesh). Several grids were used, including 20.000, 40.000, and 100.000 nodes, and the mesh is very refined near the heated wall to capture the maximum amount of data for the various depth values (Figure 5).

Mesh Sensivity

Three structured grids are tested to examine mesh quality and its impact on simulation calculations. As illustrated in Figure 6, the mesh number ranged from 20,000 to 100,000 nodes. The three curves are found to have the same profile as the experimental data. The temperature varies significantly along the kiln; the first grid (20,000 nodes) represents a good compromise between result accuracy and computational cost and time.

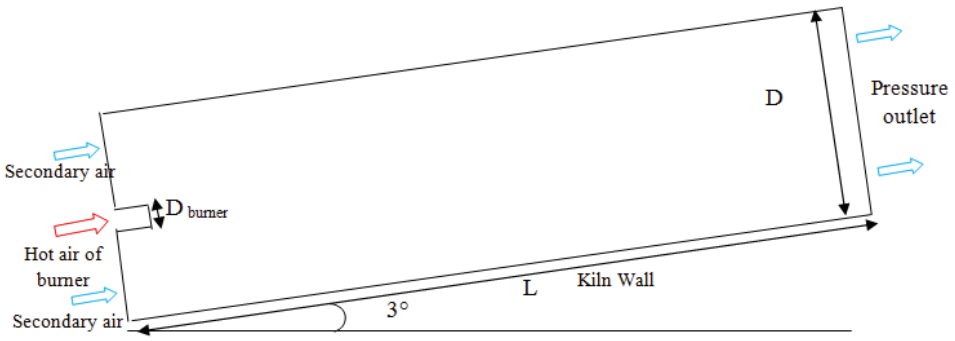

Figure 4. Schematic of studied geometry.

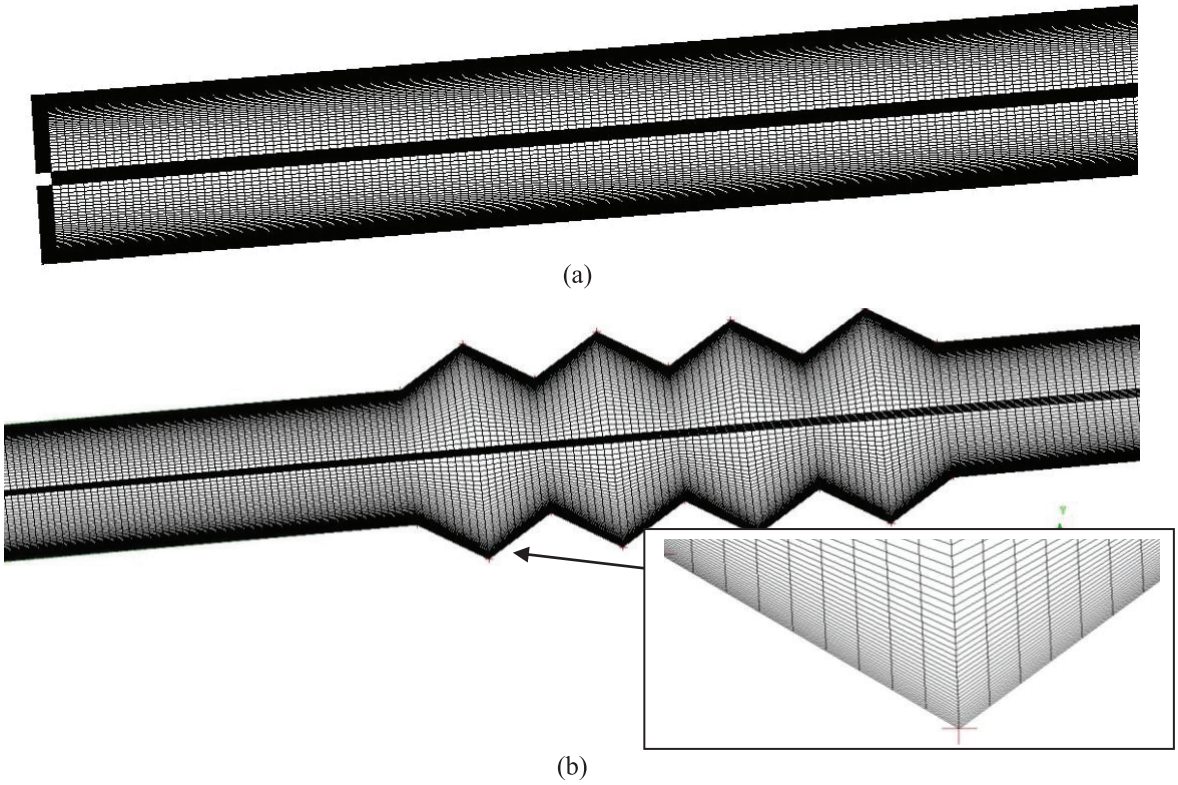

Figure 5. Grid of the computational domain: (a) smooth walls; (b) grooved walls.

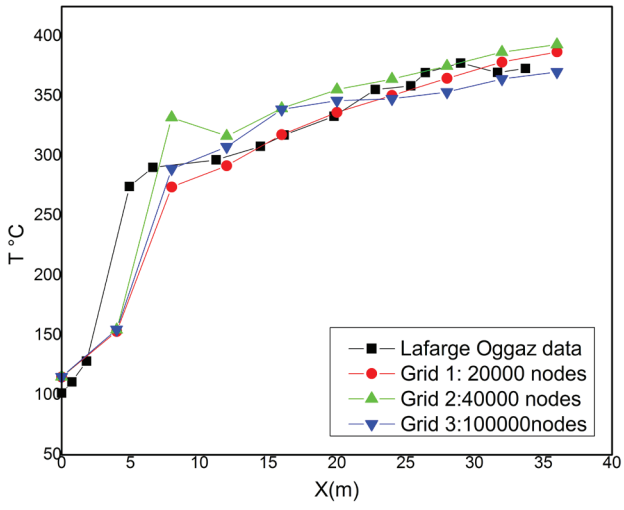

Figure 6. Mesh size effect on the temperature profiles.

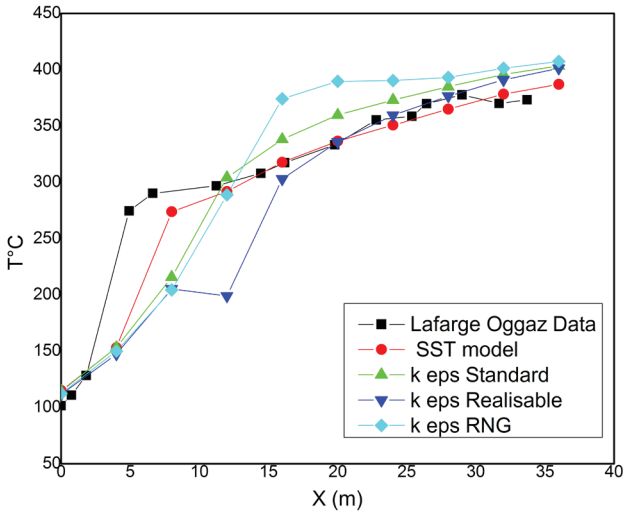

Figure 7. Turbulence model comparisons and validations.

Turbulence Model Validation

The code verification was performed based on the boundary conditions and geometry with real values used in the rotary kilns of Lafarge cement plant (Mascara, Algeria).

To ensure proper validation, we used the same grid generated by the ICEM CFD software, with 20,000 nodes retained. Figure 7 depicts the current numerical results as well as the temperature profile of the Lafarge cement plant. The graph shows that the general trend of increasing temperature T along the wall is correct. Several turbulence models are tested, including *k-ε Standard*, *k-ε RNG*, *k-ε realizable*, and the *shear-stress transport k-ω* (SST). It should be noted that all turbulence models follow the same profiles as the experimental data. As a result, there is a

good agreement between the *k-ω* SST model and the kiln temperature. Therefore, this turbulence model was used to carry out the simulation work.

ANALYSIS AND INTERPRETATION OF RESULTS

Temperature Evolution Along the Kiln Length

Figure 8 depicts the effect of groove depth mounted on the rotary kiln's outer wall on temperature profiles along the axial wall. The highest temperatures were recorded in case 1 (configuration without grooves), while the other cases had the lowest temperature profiles. It should be noted that the temperature of the four configurations with depths h/D (0.1, 0.2, 0.3, and 0.4) follows the same pattern and provides good kiln wall cooling when compared to the smooth case. Furthermore, the peaks of temperature profiles can be seen in configurations with grooves. On the other hand, the temperature rises along the groove base as a result of air recirculation (the formation of vortices) within the grooves. At (X = 35m), a temperature difference of 120 °C is observed between the grooved wall with depth (h/D = 0.4) and the smooth wall. As a result, the V-shaped configurations provide significant wall cooling to protect the external walls from deformations.

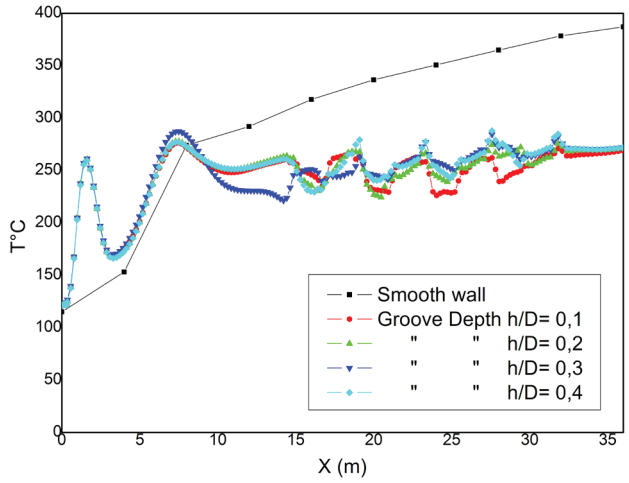

Figure 8. Temperatures evolution graph as a function of kiln length.

Local Nusselt Number Evolution

Figure 9 depicts four grooved channel configurations as well as a smooth channel.

This figure illustrates the same evolution of Nusselt number profiles. In contrast to the smooth walls, the four graphs that include grooves with different depths (h/D=0.1, 0.2, 0.3, and 0.4) show a significant increase in Nusselt number. Furthermore, the presence of grooves on the burning part can be used to achieve the peaks (15-32m). Increases in groove depth h result in greater heat exchange enhancement due to an increase in the size of the recirculation zone. The grooved wall with h/D=0.4 has the highest Nu on the kiln burning part (Nu=1700), while the smooth wall case has the lowest Nu (Nu=600).

Variation of the Local Friction Coefficient Cf

The variation of the friction coefficient C_f along the axial wall of the rotary kiln for different groove depths (h/D=0.1, 0.2, 0.3, and 0.4) is shown in Figure 10. It can be seen that the amplitudes (h/D=0.2, 0.3, and 0.4) have the same evolution along the wall as the flat wall. The C_f coefficient decreases from (C_f =0.17) at the kiln's inlet to (C_f=0.005) at position (X=10m) then we see the appearance of the peaks for each groove. We also notice that as the depth of the groove increases, so does the C_f. As can be seen, the highest values of C_f are found at the kiln burning part (C_f =0.06), particularly at the top of the V-shaped grooves where the flow is recirculated.

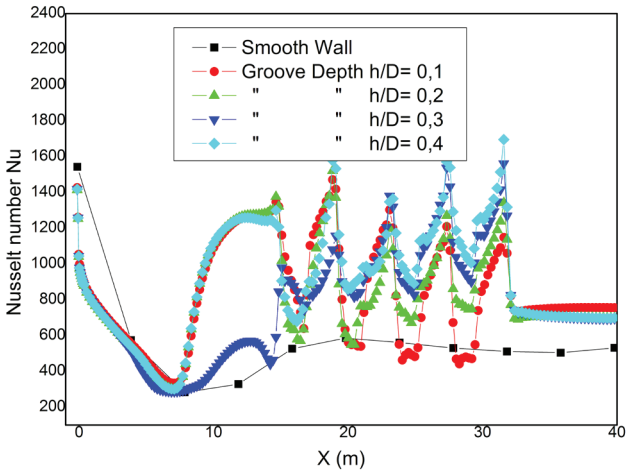

Figure 9. Local Nusselt number versus kiln length for different grooves depth.

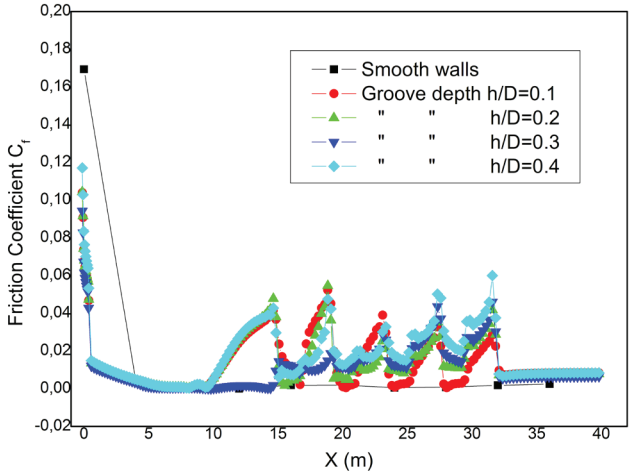

Figure 10. local friction coefficients versus kiln length for different grooves depth.

Temperature Contours

Figure 11 shows the effect of mounting different V-shaped groove depths on the temperature distribution in a rotary kiln. According to the temperature contours, the high temperature zone area is located near the burner, and the maximum air temperature produced by the burner is (T=1573K), as shown in figure 11. It is also discovered that the lowest temperature values are found inside the grooves. As a result of the creation of a recirculation zone inside the fins, the V-shaped grooves improve air mixing near the wall, particularly for the fourth and fifth configurations (h/D=0.3 and 0.4). Therefore, increasing the groove depth lowers the temperature of the kiln walls.

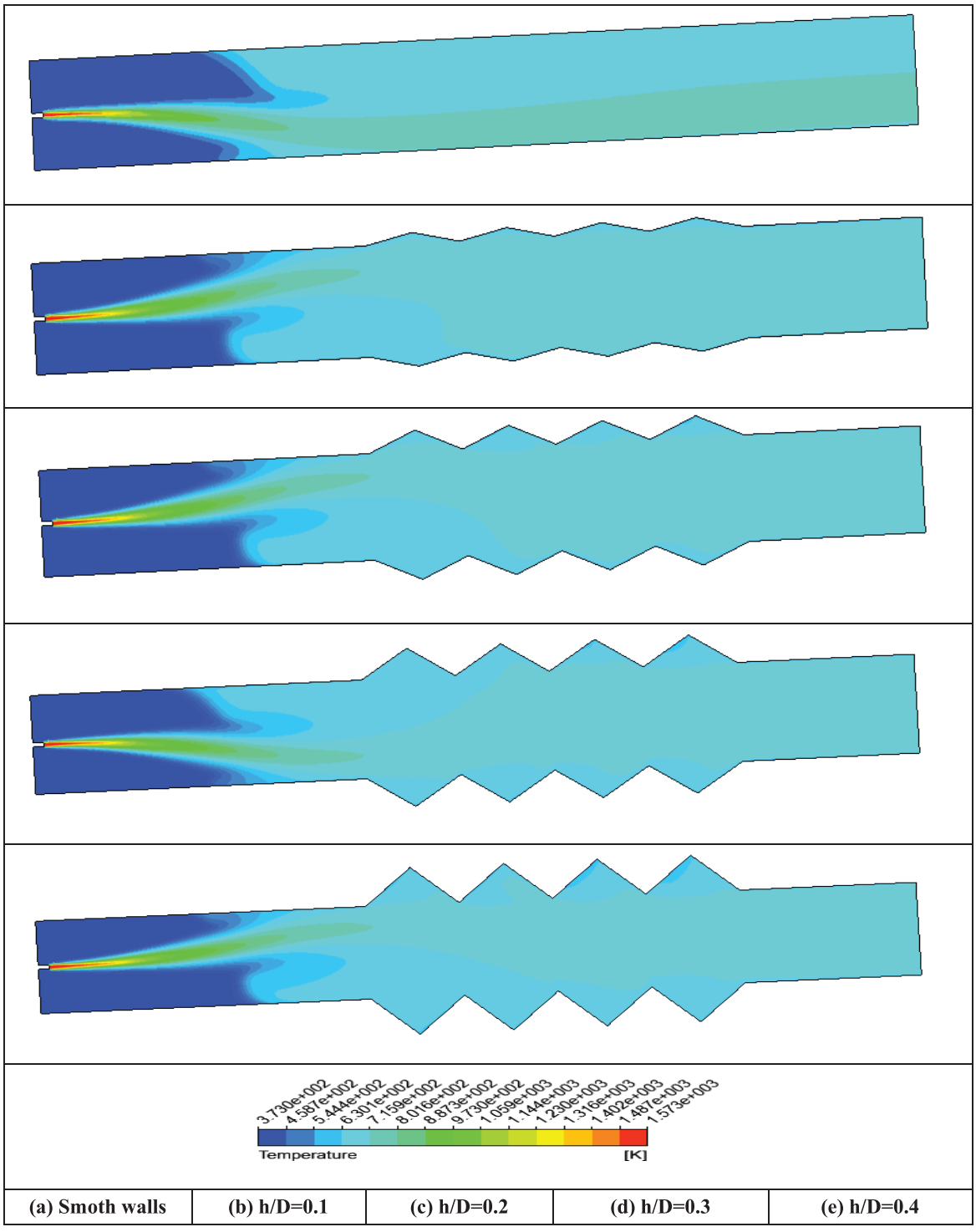

Figure 11. Isotherm contours of rotary kiln at different groove depths.

Streamline Contours

Figure 12 depicts velocity pathlines within the rotary kiln for each of the five configurations with and without V-shaped grooves. Because of the high velocity and temperature of the primary air, the air flow is deflected away from the burner, producing a large turbulence that is filled with hot air and distributed along the kiln wall, according to the streamlines. It is also shown that the air inside the grooved channel is distinguished by the presence of a recirculation zone formed within each groove along the longitudinal axis. Furthermore, as seen in the streamlines plot, the growth of the recirculation region inside the groove increases with increasing groove depth from h/D=0.1 to 0.4 and it is well distributed, particularly for the fourth and fifth configurations.

CONCLUSION

The work discussed in this paper enabled the use of a commercial CFD code to study the numerical simulation of the forced convection of a turbulent flow over grooved walls of a rotary cement kiln. The results are obtained by the computational simulation of cooling the rotary kiln's outer wall through four grooved configurations.

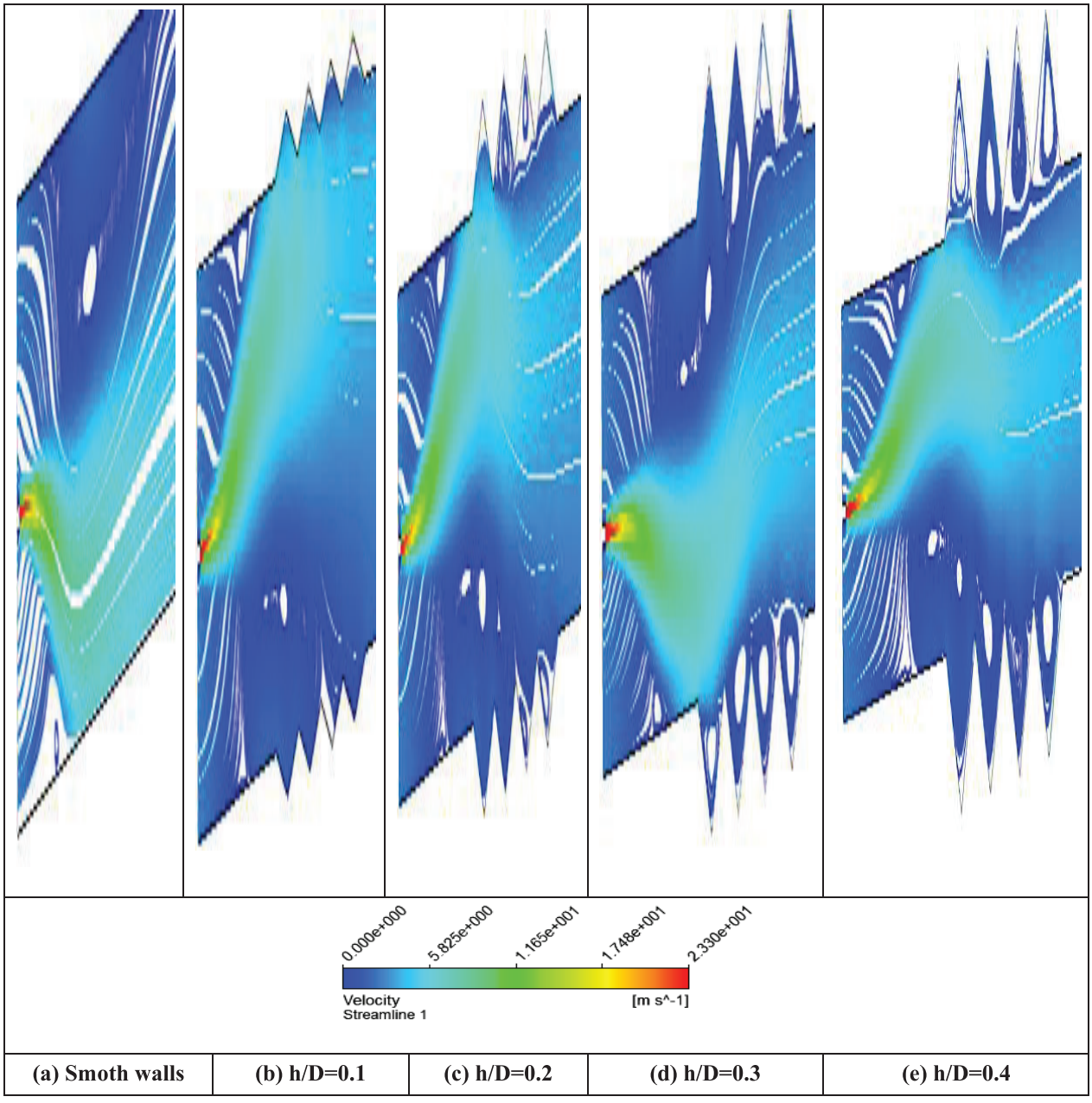

Figure 12. Streamlines of air velocity for different groove depths.

The numerical results presented in this study demonstrate that the use of V-shaped grooves mounted on the burning part of the rotary kiln contributes to a consequent heat exchange, with the effects of this improvement visible in the Nusselt number and temperature profiles, which increase in value when compared to the smooth kiln wall. According to the findings of this study, the grooved channel with depths h/D=0.3 and 0.4 provides significant wall cooling and significantly higher turbulence than the other cases to protect the rotary kiln's outer walls from deformations.

NOMENCLATURE

L	Length of the kiln, [m]
D	Kiln diameter, [m]
d	Burner diameter, [m]
T	Temperature, [K]
d_h	hydraulic diameter , [m]
V	axial speed of fluid, [$m.s^{-1}$]
Nu	Nusselt number
C_f	Coefficient of friction
k	Turbulence kinetic energy, [$m^2.s^{-2}$]
h	Convective heat transfer coefficient, [$W.m^{-2}.K^{-1}$],

Greek symbols

ρ	Fluid density, [kg/m^3]
λ	Thermal conductivity, [$W.m^{-1}. K^{-1}$]
ν	Kinematic viscosity, [$m^2.s^{-1}$]
ε	Turbulence dissipation rate, [$m^2.s^{-3}$]
ν_t	Turbulent kinematic viscosity, [$m^2.s^{-1}$]
τij	Viscous stress tensor
δ_{ij}	Kronecker delta
ϕ	Generalized variable
ω	Specific dissipation rate, [s^{-1}]

AUTHORSHIP CONTRIBUTIONS

Authors equally contributed to this work.

DATA AVAILABILITY STATEMENT

The authors confirm that the data that supports the findings of this study are available within the article. Raw data that support the finding of this study are available from the corresponding author, upon reasonable request.

CONFLICT OF INTEREST

The author declared no potential conflicts of interest with respect to the research, authorship, and/or publication of this article.

ETHICS

There are no ethical issues with the publication of this manuscript.

REFERENCES

[1] Peray KE, Waddell JJ. The Rotary Cement Kiln. New York: Chemical Publishing Co., Inc.; 1972:71−77.

[2] Gorg JP, Brimacombe JK. Radiative heat transfer in rotary transfer in rotary kilns. Metallurgical Tran B 1981;12B:55−64. [CrossRef]

[3] Bui RT, Perron J, Read M. Model-based optimization of the operation of the coke calcining kiln. Carbon 1993;31:1139−1147. [CrossRef]

[4] Sass A. Simulation of the heat transfer phenomenon in a rotary kiln. Ind Eng Chem Proc Des Dev 1967;6:532−535. [CrossRef]

[5] Ghoshdastidar PS, Bhargava G, Chhabra RP. Computer simulation of heat transfer during drying and preheating of wet iron ore in a rotary kiln. Drying Technol 2002;20:19−35. [CrossRef]

[6] Ghoshdastidar PS, Agarwal A. Simulation and optimization of drying of wood chips with superheated steam in a rotary kiln. J Therm Sci Eng Appl 2009;1:024501. [CrossRef]

[7] Schmidt R, Nikrityuk PA. Numerical simulation of the transient temperature distribution inside moving particles. Can J Chem Eng 2012;90:246−262. [CrossRef]

[8] Sonavane Y, Specht E. Numerical analysis of the heat transfer in the wall of rotary kiln using finite element method ANSYS. Proceedings of 7th International Conference on CFD in the Minerals and Process Industries 2009; CSIRO, Melbourne, Australia.

[9] Cook CA, Cundy VA. Heat transfer between a rotating and a moist granular bed. Int J Heat Mass Transfer 1995;38:419−432. [CrossRef]

[10] Elattar HF, Stanev R, Specht E, Fouda A. CFD simulation of confined non-premixed jet flames in rotary kilns for gaseous fuels. Comput Fluids 2014;102:62−73. [CrossRef]

[11] Elattar HF, Specht E, Fouda A, Bin-Mahfouz AS. Study of parameters influencing fluid flow and wall hot spots in rotary kilns using CFD. Can J Chem Eng 2016;94:355−367. [CrossRef]

[12] Mirhosseini M, Rezaniakolaei A, Rosendahl L. Numerical study on heat transfer to an arc absorber designed for a waste heat recovery system around a cement kiln. Energies 2018;11:1−16. [CrossRef]

[13] Singh D, Premachandran B, Kohli S. Experimental and numerical investigation of jet impingement cooling of a circular cylinder. Int J Heat Mass Transf 2013;60:672−688. [CrossRef]

[14] Ayadi B, Selimefendigil F, Alresheedi F, Kolsi L, Aich W, Said LB. Jet impingement cooling of a rotating hot circular cylinder with hybrid nanofluid under multiple magnetic field effects. Mathematics 2021;9:2697. [CrossRef]

[15] Csernyei C, Straatman AG. Forced convective heat transfer on a horizontal circular cylinder due to multiple impinging circular jets. Appl Therm Engineer 2016. [CrossRef]

[16] Attou Y, Dellil AZ, Meghdir A. Impact of the grooves on the enhancement of heat transfer in an annular space of a rotor-stator. Int J Heat Technol 2018;36:1283−1291. [CrossRef]
[17] Kebir F, Attou Y. Scrutiny the heat transfer effect in an annulus by mounting axial fins with different shapes: Without and with taylor number. Defect Diffusion Forum 2021;409:142−157. [CrossRef]
[18] Attou Y, Kebir F. Effect of fin inclination angel on heat transfer improvement in an annular space of a rotor stator. Defect Diffusion Forum 2021;409:110−122. [CrossRef]
[19] Nouri-Borujerdi A, Nakhchi ME. Friction factor and Nusselt number in annular flows with smooth and slotted surface. Heat Mass Transf 2018;55:645−653. [CrossRef]
[20] Nouri-Borujerdi A, Nakhchi ME. Experimental study of convective heat transfer in the annulus of an annulus with an external grooved surface. Exp Thermal Fluid Sci 2018;98:557−562. [CrossRef]
[21] Gkiokchan M, Stefania Tescari A, Christian Sattler AB. Impact of bed motion on the wall-to-bed heat transfer for powders in a rotary kiln and effect of built-ins. Int J Heat Mass Transf 2021;177. [CrossRef]
[22] Lafarge. La cimenterie Lafarge Ciment Oggaz. Available at: https://www.lafarge.dz/1_2_2_2-usine_d_oggaz.
[23] Patankar S, Spalding DA. Computation procedure for heat, mass and momentum transfer in three-dimensional parabolic flows. Int J Heat Mass Transf 1975;15:1787−1806. [CrossRef]
[24] Fluent, Inc., Turbulence Modelling, Fluent 6.1 Documentation, Chapters 7, 9, 12, and 13. 2003.
[25] Menter FR. Two-equation eddy-viscosity turbulence models for engineering applications. AIAA J 1994;32:1598−1605. [CrossRef]
[26] Wilcox DC. Turbulence Modeling for CFD Second Edition. D.C.W. Industries; 1998.
[27] Jones W, Launder B. The calculation of low-Reynolds-number phenomena with a two-equation model of turbulence. Int J Heat Mass Transf 1973;16:1119−1130. [CrossRef]
[28] Bardina JE, Huang PG, Coakley TJ. Turbulence modeling validation, testing, and development. NASA Technical Memorandum; 1997. [CrossRef]
[29] Csernyei C, Straatman AG. Numerical modeling of a rotary cement kiln with improvements to shell cooling. Int J Heat Mass Transf 2016;102:610−621. [CrossRef]
[30] Ao C, Yana S, Hua W, Zhaoa L, Wu Y. Heat transfer analysis of a PCM in shell-and-tube thermal energy storage unit with different V-shaped fin structures. Appl Therm Engineer 2022;216. [CrossRef]
[31] He J, Deng Q, Xiaoa K, Feng Z. Heat transfer enhancement by V-shaped protrusions on jet plate under different crossflow conditions. Int Comm Heat Mass Transf 2023;141. [CrossRef]
[32] Shashikumar CM, Madav V. Performance analysis of novel V-shaped turbine blade profile by three-dimensional numerical investigations with varying overlap ratios for hydropower application. Ocean Engineer 2022;265. [CrossRef]
[33] Promvonge P, Tongyote P, Skullong S. Thermal behaviors in heat exchanger channel with V-shaped ribs and grooves. Chem Engineer Res Design 2019;150:263−273. [CrossRef]
[34] Kaur I, Singh P. Heat and flow characteristics of V-shaped protrusion/concavity combined with miniature V-ribs. Numer Heat Transf. A Appl 2020:1−19. [CrossRef]